

Design and Evaluation of a Stochastic Optimal Feed-Forward and Feedback Technology (SOFFT) Flight Control Architecture

Aaron J. Ostroff
Langley Research Center • Hampton, Virginia

Melissa S. Proffitt
Lockheed Engineering & Sciences Company • Hampton, Virginia



Contents

Abstract	1
Introduction	1
Background	1
Nomenclature	3
SOFFT Feed-Forward Controller	4
Command Model	5
Plant Model	7
Plant-model interpolation	7
Plant-model dynamics	8
Feed-Forward Gains	8
Algorithm	9
Feedback Controller	9
Facilities	11
Simulation Results and Discussion	11
Feedback Controller Specifics	12
Agility	12
Tracking	13
Concluding Remarks	14
References	15

Abstract

This paper describes the design and evaluation of a stochastic optimal feed-forward and feedback technology (SOFFT) control architecture with emphasis on the feed-forward controller design. The SOFFT approach allows the designer to independently design the feed-forward and feedback controllers to meet separate objectives and then integrate the two controllers. The feed-forward controller has been integrated with an existing high-angle-of-attack (high- α) feedback controller. The feed-forward controller includes a variable command model with parameters selected to satisfy level 1 flying qualities with a high- α adjustment to achieve desired agility guidelines, a nonlinear interpolation approach that scales entire matrices for approximation of the plant model, and equations for calculating feed-forward gains developed for perfect plant-model tracking. The SOFFT design was applied to a nonlinear batch simulation model of an F/A-18 aircraft modified for thrust vectoring. Simulation results show that agility guidelines are met and that the SOFFT controller filters undesired pilot-induced frequencies more effectively during a tracking task than a flight controller that has the same feedback control law but does not have the SOFFT feed-forward control.

Introduction

Typically, control designers try to achieve different, and sometimes conflicting, design objectives. Examples of these control objectives include the following: (1) good closed-loop stability characteristics (damping and bandwidth), (2) desired response to pilot input commands (flying qualities), (3) quick response to pilot input commands during large amplitude maneuvers (transient response), (4) maintenance of stability and tracking performance despite system uncertainties and various nonlinearities (robustness), (5) attenuation of high-frequency disturbances and measurement noise, and (6) accommodation of low-frequency plant disturbances.

Modern optimal control designs that attempt to meet many of these requirements with only a single cost function place conflicting demands on the controller. For example, when the single cost function is optimized to provide good tracking characteristics, the controller usually has a high bandwidth with large feedback gains and poor noise attenuation.

The SOFFT (stochastic optimal feed-forward and feedback technology) approach separates the feed-forward and feedback control objectives. The feedback controller and the feed-forward controller are then designed with different cost functions. Control objectives such as 2, 3, and 4 that relate system response to pilot input commands are met by the feed-forward controller. Control objectives such as 1, 4, 5 and 6 that relate to closed-loop damping and stability, bandwidth, plant disturbance accommodation, and external noise reduction are met by the feedback

controller. After the designs are completed, the feed-forward and feedback controllers are integrated with the SOFFT control structure to best meet all control objectives. A particular incremental implementation (described subsequently in this paper) is applied to the integrated controllers. This implementation allows control objective 6 to be met and avoids the need for operating point trim schedules.

This paper describes the design for a SOFFT feed-forward controller that is integrated with an existing high angle-of-attack (high- α) feedback controller. The feed-forward controller includes (1) a variable command model with level 1 flying qualities and with a high- α adjustment to achieve agility guidelines, (2) a unique interpolation approach that scales entire matrices for approximation of the plant model, and (3) equations for calculating feed-forward gains developed for perfect tracking. The nonlinear batch simulation includes results for agility performance and tracking.

Background

Significant technical advancements in modern control theory have occurred during the past two decades. This section contains a summary of previous research efforts that have influenced the direct digital control design described in this paper and the SOFFT (stochastic optimal feed-forward and feedback technology) methodology (ref. 1). These previous research efforts illustrate continuous technological improvements leading to a direct digital modern control design approach that is being used in a practical airplane control design application.

During the mid to late 1970's, a digital flight control system (refs. 2 and 3) was developed for use on the VALT (VTOL approach and landing technology) CH-47B research aircraft. The key technologies included a full-state direct digital design for inner-loop control, a PIF (proportional integral filter) control structure, and an incremental implementation for the digital flight computers. The main disadvantage of this technology was that the full-state control design required state estimators for feedback. In addition, complex gain-scheduling techniques were used to make the control system operational over a wide flight envelope. To demonstrate these methodologies, a command generator and outer-loop controller were designed around the inner-loop PIF controller. The CH-47B aircraft then flew automatically along a curved four-dimensional trajectory to a hover and finally descended vertically to a landing (ref. 4).

During the late 1970's, the DIALS (digital integrated automatic landing system) control law was developed (ref. 5). DIALS was a full-state feedback design that required a full-state estimator. Because the application was for a limited flight envelope, only a single point design was used; thus, ad hoc gain-scheduling techniques that would have been required for a larger flight envelope were avoided. This control methodology was flight tested on the Boeing 737 research airplane at Langley during the early 1980's (refs. 6 and 7). A constant-gain feedback matrix was used because automatic landing, which results in relatively constant flight conditions, was the overall control objective of the flight test. Also, trim values for the steady-state operating condition were required because the control methodology was a full-state design that was implemented in perturbational form.

A discrete, optimal output, feedback algorithm was developed during the early 1980's (refs. 8 and 9). This algorithm was an improvement over VALT and DIALS because the feedback controller only needed measured signals instead of the full-state feedback. A key advantage of this algorithm was that all important dynamics such as actuators, sensors, and filters could be included in the design process. A disadvantage is that the optimal output feedback technique was still a single point design approach, and ad hoc gain-scheduling techniques were still required. This technology, including the PIF controller with the incremental control structure, was used in restructurable controls research applications (refs. 10 to 12) in which control effectors were reconfigured to accommodate failures, and it was used in wind shear penetration research during the approach and landing phases of flight (ref. 13). For all these appli-

cations, nonlinear batch simulation of the Boeing 737 at Langley was used as the test bed.

During the mid 1980's, an algorithm for multi-model output feedback was developed (ref. 14). The objective was to improve control design robustness by specifying different models around the same operating point and by designing a fixed-gain output feedback matrix that satisfied all models. With this algorithm, the control system should be robust enough to handle many different parameter variations.

The multimodel methodology led to the next major advancement during the late 1980's when the variable-gain output feedback methodology was developed (refs. 15 and 16). This methodology allows simultaneous processing of multiple design points over the complete flight envelope, thus creating a more efficient design tool. The design algorithm generates feedback gains that, in combination with a priori selected scalar design parameters, create an optimal gain schedule. The variable-gain technique is a modern control approach that can be used in a practical airplane control design application; however, specifications for flying qualities cannot be directly incorporated into the methodology.

Variable-gain control was first applied to reconfigurable aircraft (ref. 17), where gain-scheduling parameters were functions of the percentage loss of control effectors. Recent applications were for airplane up-and-away flight (refs. 18 and 19). The feasibility of using the variable-gain output feedback methodology was established by using four design conditions and one gain-scheduling parameter for high- α flight at constant altitude (ref. 18). An expanded case with 39 design conditions and 6 gain-scheduling parameters was used to design a feedback controller that covered the HARV (high-angle-of-attack research vehicle) flight envelope (refs. 19 and 20). The HARV (ref. 21) is an F/A-18 aircraft that has been modified to include thrust vectoring. The controller described in reference 19 has been tested in real-time piloted simulation and is scheduled for flight test. This controller is used in the SOFFT feedback system described in this paper.

Some research on explicit model following is germane to the SOFFT approach. Explicit model following was one of the techniques investigated on an unstable advanced fighter model (ref. 22). A single quadratic cost function was used to minimize the error between the aircraft response and the command-model response. This controller had high gains and correspondingly high controller bandwidth, both of which resulted in excessive actuator rates. These results are typical of explicit model following

techniques that use a single cost function. Another method used explicit model following but had separate designs for the feed-forward and feedback controllers (ref. 23). This approach allowed the feed-forward controller bandwidth to be tailored independent of the feedback controller bandwidth to meet flying qualities objectives.

Finally, during the early 1990's, the SOFFT technology was developed (ref. 1). SOFFT is a design methodology that uses a unique control structure for integrating the feed-forward and feedback controllers and is applicable to multiple design points over the complete flight envelope. Also, flying qualities can be incorporated into the control design. A controller using the SOFFT methodology has been designed for application to a model of an HARV airplane. This controller incorporates many of the features described in previous references, such as (1) direct digital design, (2) PIF control architecture, (3) incremental implementation, (4) variable-gain feedback design, and (5) separation of designs for the feed-forward and feedback controllers. This configuration was recently tested in a nonlinear batch simulation and is the subject of this paper.

Nomenclature

Notation used in this paper includes boldface symbols for matrices and vectors and italicized symbols for scalars.

\mathbf{A}_z	command-model continuous-state matrix	\mathbf{H}_y	matrix used to select regulated outputs
\mathbf{B}_z	command-model continuous-control matrix	h	height
C_N	normal-force coefficient	\mathbf{I}	identity matrix
$C_{N\alpha}$	variation of normal-force coefficient C_N with α , rad^{-1}	K_u	command-model control input gain
\mathbf{C}_x^*	interpolated plant-model state to output matrix	K_x^*	plant-model state gains
\mathbf{C}_z	command-model output matrix	K_{xI}	integrator gain in feedback controller
\bar{c}	mean aerodynamic chord	K_{xu}	control filter gain in feedback controller, sec^{-1}
CAP	control anticipation parameter	\mathbf{K}_{xx}	proportional feedback gain matrix
\mathbf{D}_x^*	interpolated plant-model control to output matrix	\mathbf{K}_z	command-model state gain matrix
e^*	feed-forward command tracking error	k	coefficient for sampling sequence at time t_k
\mathbf{H}_x^*	plant-model state to regulated variable output transfer matrix	M	number of plant models
		n	number of models used in scaling plant matrices
		n_p	number of gain-scheduling parameters
		n_z	normal acceleration, g units
		$n_{z,c}$	load-factor command, g units
		$n_{z,ss}$	steady-state normal acceleration, g units
		P_s	static pressure, lbf/ft^2
		p	parameter representing measured variables
		$\bar{\mathbf{p}}$	vector of measured parameters
		$\bar{\mathbf{p}}^j$	vector of parameters for each of the plant models
		Q_c	impact pressure, lbf/ft^2
		q	pitch rate, deg/sec
		\dot{q}	pitch acceleration, deg/sec^2
		\bar{q}	dynamic pressure, lbf/ft^2
		S	reference wing area, ft^2
		s	Laplace variable
		u_x	control position command in feedback controller, deg
		\mathbf{u}_x^*	ideal plant-model control trajectory, deg
		u_z	command input to SOFFT feed-forward controller

\tilde{v}_x	rate command in feedback controller
W	weight of airplane, lbf
\mathbf{x}^*	plant-model state vector
\mathbf{x}_z	command-model state vector
y_{cx}^*	ideal command to feedback controller
\mathbf{y}_x	output feedback measurement vector
\mathbf{y}_x^*	ideal plant output trajectory
\tilde{y}_x	feedback controller error signal
y_z	command-model output
z	z -transform variable
α	angle of attack, deg
α_c	angle-of-attack command, deg
Γ_x^*	interpolated plant discrete control matrix
Γ_z	command-model discrete control matrix
ΔT	discrete sampling period, sec
Δu_x^*	incremental plant-model control, deg
Δu_z	incremental command-model input
$\Delta \mathbf{x}_z$	incremental command-model state vector
$\Delta \mathbf{x}^*$	incremental plant-model state vector
Δy_x	incremental output feedback measurements
Δy_x^*	incremental plant-model output
δ_{sp}	pilot pitch stick input command, in.
ζ_z	command-model short-period damping ratio
$\ddot{\theta}_0$	initial pitch acceleration, rad/sec ²
ν_i	variable for gain-scheduling parameter selected by designer
$\bar{\rho}$	scaling parameter
ρ_j	distance in parameter space from operating point to each plant model
Φ_x^*	interpolated plant discrete state transition matrix

Φ_z	command-model discrete state transition matrix
ϕ_x^*	interpolated matrix
ω_{sp}	short-period frequency, rad/sec
ω_z	command-model short-period frequency, rad/sec
Subscript:	
k	coefficient for sampling sequence at time t_k

Abbreviations:

DIALS	digital integrated automatic landing system
HARV	high-angle-of-attack research vehicle
PI	proportional plus integral structure
PIF	proportion integral filter
SOFFT	stochastic optimal feed-forward and feedback technology
VALT	VTOL approach and landing technology
VTOL	vertical take-off and landing

SOFFT Feed-Forward Controller

The complete feed-forward controller has two main components: the command generator with selectable modes and the SOFFT feed-forward controller (fig. 1). Pilot pitch stick input commands δ_{sp} go directly to the command generator, which scales the inputs based upon stick sensitivity, mode, and flight-operating conditions. Signals are calculated for two modes: a load-factor command mode $n_{z,c}$ and an angle-of-attack command mode α_c . The mode selector then chooses the smaller of the two signals for the output command u_{zk} . Selection of the smallest signal gives the best solution for the operating region of interest because each of the feed-forward gains can become large at different parts of the flight envelope. A derivation and implementation for the command generator with mode selection is presented in references 19 and 20. The methodology used in the references does not have a direct approach for incorporating flying qualities guidelines.

The SOFFT feed-forward controller converts command u_{zk} into ideal trajectory commands for the control \mathbf{u}_{xk}^* and ideal plant output \mathbf{y}_{xk}^* , both of which are sent to the feedback controller. In this paper, the subscript k represents the coefficient

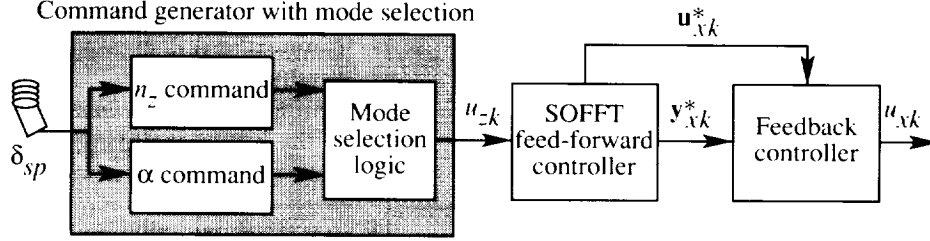


Figure 1. Complete feed-forward control system.

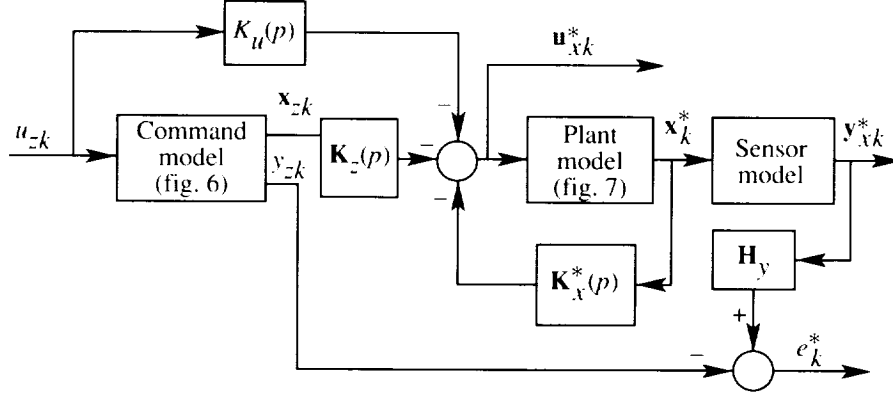


Figure 2. SOFFT feed-forward controller structure.

for the sampling sequence at time t_k and the asterisk represents ideal trajectory variables with the assumption that the plant model represents the actual model. Figure 2 is a block diagram of the SOFFT feed-forward controller structure. The main components are the command model, plant model, and feed-forward gains. These components are described in the following subsections.

Command Model

The command model incorporates variable dynamics, where short-period frequency and damping are based upon the guidelines for level 1 flying qualities (ref. 24). An important flying qualities variable is the control anticipation parameter CAP , which is defined as the ratio of initial pitch acceleration $\ddot{\theta}_0$ to the steady-state normal acceleration $n_{z,ss}$:

$$CAP = \frac{\ddot{\theta}_0}{n_{z,ss}} \approx \frac{\omega_{sp}^2}{n_z/\alpha} \quad (1)$$

CAP is approximated as the ratio of the square of the short-period frequency ω_{sp} to the ratio n_z/α . The ratio n_z/α can be expressed as

$$\frac{n_z}{\alpha} = \frac{C_{N_\alpha} \bar{q} S}{W} = \frac{C_{N_\alpha} \bar{q}}{89.413} \quad (2)$$

where C_{N_α} is the variation of the normal-force coefficient C_N with α , \bar{q} is the dynamic pressure, S is the reference wing area (400 ft²), and W is the weight of the airplane (35 765 lbf). The calculation of CAP is used extensively at low α , but it is not a useful flying qualities metric at high α , where the airplane is in the stall region. Values of CAP that vary between 0.28 and 3.6 meet the guidelines for level 1 flying qualities. Figure 3 illustrates the relationship between CAP , ω_{sp} , and the ratio n_z/α and shows the region for level 1 flying qualities. The design parameters for the command model are located along the upper boundary of the level 1 region, with a lower boundary of 3 for the command-model short-period frequency ω_z . The lower boundary of 3 was chosen to meet agility guidelines; related experimental results are shown later in the section entitled "Agility." Figure 4 shows a plot of C_N as a function of α with approximate values of slope C_{N_α} located in the appropriate locations. The simulation model for C_{N_α} is implemented by an upper boundary of 5.3 rad⁻¹ for $\alpha < 7.5^\circ$, a lower boundary of 2.4 rad⁻¹ for $\alpha > 17.5^\circ$, and a straight line between. The C_N was calculated from lift and drag coefficients, which were available at all trim conditions in our data base.

At low \bar{q} and high α (above 30°), ω_z was modified to be

$$\omega_z = (0.6 + 0.08\alpha) \frac{1.2}{n_z/\alpha} \quad (3)$$

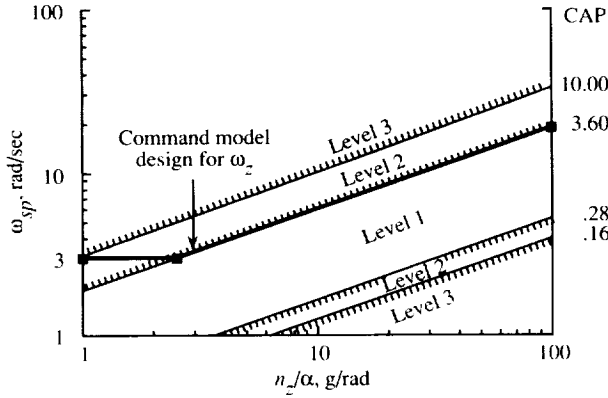


Figure 3. Short-term pitch response command. (From ref. 24.)

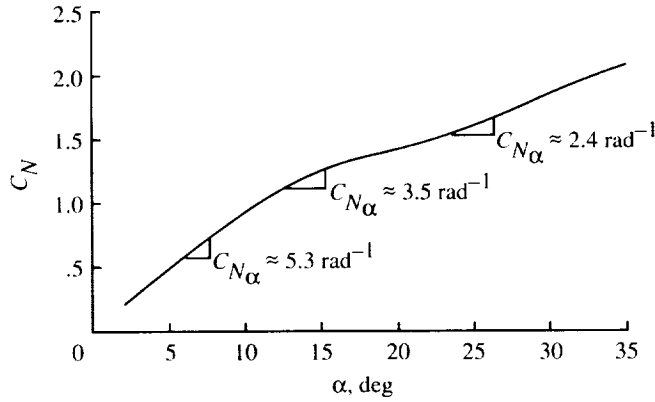


Figure 4. Normal-force coefficient as a function of α .

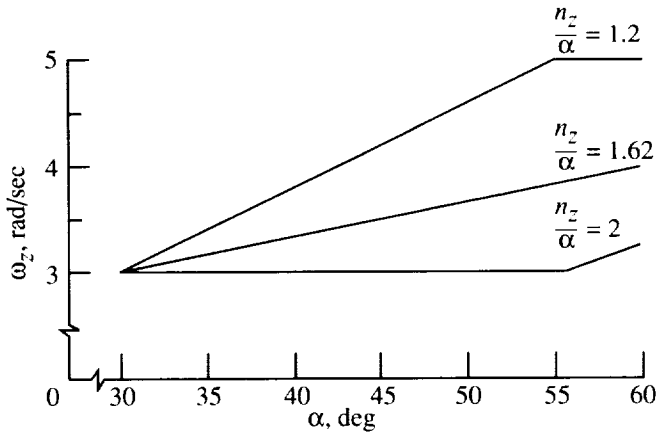


Figure 5. Low-speed high- α adjustment.

with a lower boundary of 3 and an upper boundary of 5. As an example, the upper boundary can occur when α is 55° or greater and n_z/α is 1.2 or less,

whereas the lower boundary can occur when either n_z/α increases or α decreases. The smaller values for n_z/α usually occur at high α where both $C_{N\alpha}$ and \bar{q} are small. Equation (3) was derived experimentally to meet the high- α agility guidelines. Figure 5 is a plot illustrating this adjustment.

Figure 6 shows the complete command-model configuration. Two items not previously discussed are the command-model short-period damping ratio ζ_z and the discrete dynamic model. The value of ζ_z varies between 0.71 at high-speed conditions ($n_z/\alpha = 10$) and 1.0 at low-speed conditions ($n_z/\alpha = 1.1$). The reason for this adjustment is because recent research shows that pilots prefer high damping at high- α flight conditions (ref. 25).

The command model has second-order dynamics as shown by the transfer function

$$\frac{y_{zk}}{u_{zk}} = \frac{\omega_z^2}{s^2 + 2\zeta_z\omega_z s + \omega_z^2} \quad (4)$$

where the variables ω_z and ζ_z vary with parameter p (representing α and \bar{q} in this case) as flight conditions change. Equation (4) is transformed to a discrete state-space representation

$$\left. \begin{aligned} \mathbf{x}_z(p, k+1) &= \Phi_z(p) \mathbf{x}_z(p, k) + \Gamma_z(p) u_z(p, k) \\ y_z(p, k) &= \mathbf{C}_z(p) \mathbf{x}_z(p, k) \end{aligned} \right\} \quad (5)$$

where \mathbf{x}_z is the command-model state vector, u_z is the command-model input (single command), Φ_z is the command-model discrete state transition matrix, Γ_z is the command-model discrete control matrix, \mathbf{C}_z is the command-model output matrix, and integer k represents the sample at time t_k . Matrices $\Phi_z(p)$, and $\Gamma_z(p)$ must be calculated at each iteration (\mathbf{C}_z is a constant matrix for the selected implementation) and are approximated as

$$\begin{aligned} \Phi_z(p) &= \exp[\Delta T \mathbf{A}_z(p)] \approx \mathbf{I} + \Delta T \mathbf{A}_z(p) \\ &\quad + \frac{(\Delta T)^2 \mathbf{A}_z^2(p)}{2} \end{aligned} \quad (6)$$

$$\Gamma_z(p) = \mathbf{A}_z^{-1}(p) [\Phi_z(p) - \mathbf{I}] \mathbf{B}_z(p) \quad (7)$$

where $\mathbf{A}_z(p)$ and $\mathbf{B}_z(p)$ are the continuous matrices corresponding to the transfer function in equation (4) and ΔT is the discrete sampling period (0.0125 sec).

Because ΔT is small, a second-order approximation in equation (6) gives sufficient accuracy. Individual elements for equations (6) and (7) are

$$\Phi_z = \begin{bmatrix} 1 - \frac{(\Delta T \omega_z)^2}{2} & \Delta T(1 - \Delta T \zeta_z \omega_z) \\ \Delta T \omega_z^2(-1 + \Delta T \zeta_z \omega_z) & 1 - 2\Delta T \zeta_z \omega_z + 2(\Delta T \zeta_z \omega_z)^2 - \frac{(\Delta T \omega_z)^2}{2} \end{bmatrix} \quad (8)$$

$$\Gamma_z = \Delta T \omega_z^2 \begin{bmatrix} 0.5\Delta T \\ 1 - \Delta T \omega_z \zeta_z \end{bmatrix} \quad (9)$$

where these elements are calculated at each time iteration and argument p is neglected for simplicity.

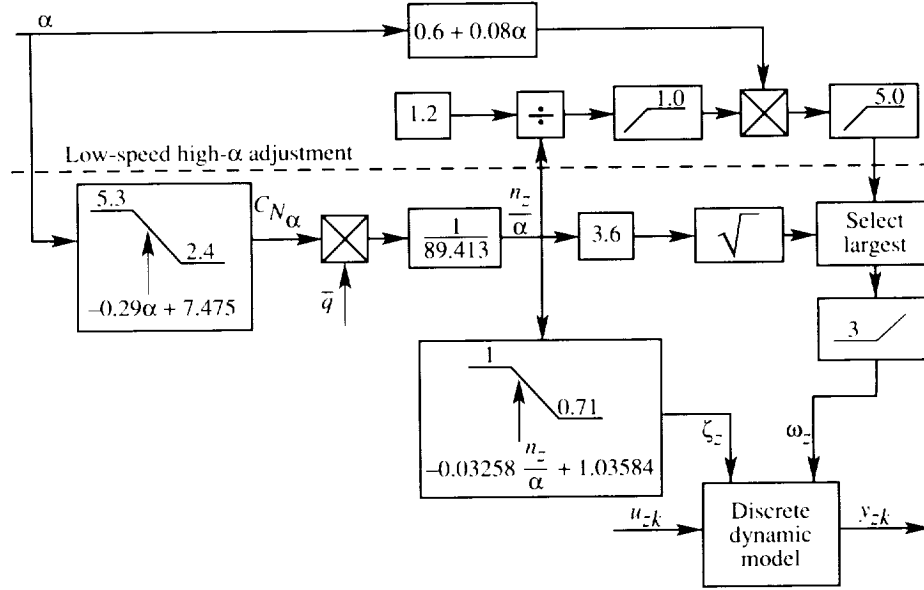


Figure 6. Command-model configuration.

Plant Model

The plant model produces the trajectory commands \mathbf{y}_{xk}^* and \mathbf{u}_{xk}^* for input to the feedback controller. To produce reasonably accurate commands, the plant model must be approximated at any flight-operating condition. Figure 7 shows the plant-model configuration and illustrates how flight-measured parameters are used to obtain matrices for the plant-model dynamics. This section described the plant-model interpolation and the plant-model dynamics.

Plant-model interpolation. In general, plant models can be composed of a series of models representing components such as actuator dynamics, airplane dynamics, sensor dynamics, and filter dynamics. Airplane dynamics change continuously with flight-operating conditions. To accommodate the complete operating range, interpolation between a finite number of specified plant models is necessary. A unique interpolation approach that scales complete

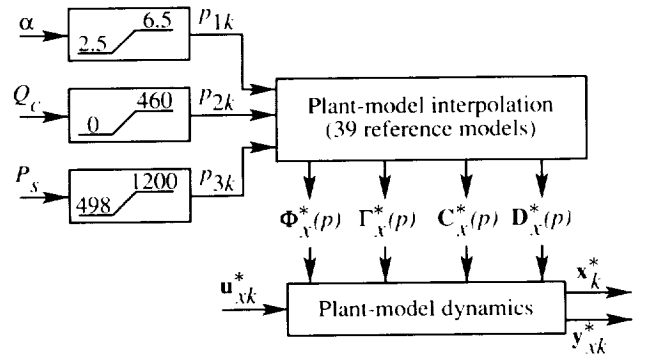


Figure 7. Plant-model configuration (perfect sensors assumed).

matrices is presented in reference 1 and is presented here for completeness. Linear interpolation is also a feasible approach, but it was not used because of time constraints and the additional complication

when more than two independent variables are used. Precise accuracy is not required for the feed-forward controller. Thus, compared with linear interpolation, the method used here is a relatively fast procedure.

A finite number of plant models are specified as a function of several parameters p that vary over the flight envelope. A metric ρ_j , representing the distance in parameter space from the operating point to each design model location, is computed as

$$\rho_j(p) = \left\| \bar{\mathbf{p}} - \bar{\mathbf{p}}^j \right\|_2 \quad (j = 1, \dots, M) \quad (10)$$

where $\bar{\mathbf{p}}$ is a vector of measured parameters that can be either linear or nonlinear, and $\bar{\mathbf{p}}^j$ is a vector of equivalent parameters for each of the M plant models. All ρ_j are sorted from smallest distance to largest distance and then the smallest n numbers are selected to be used. A scaling parameter $\bar{\rho}(p)$ is calculated by using the n closest models as follows:

$$\bar{\rho}(p) = \frac{1}{\sum_{i=1}^n \frac{1}{\rho_i(p)}} \quad (11)$$

and the ratio $\bar{\rho}(p)/\rho_i(p)$ is then used to weigh the various matrices of the n closest models as follows:

$$\phi_x^*(p) = \sum_{i=1}^n \frac{\bar{\rho}(p)}{\rho_i(p)} \phi_{xi}^*(p) \quad (12)$$

where $\phi_x^*(p)$ represents the interpolated matrix to be used for the plant model. If $\rho_i(p)$ equals 0 for any design model, then that model is used as the plant model and equations (11) and (12) are not needed.

In figure 7, p is a function of α , impact pressure Q_c , and static pressure P_s , in the design example for plant-model interpolation where each p_i is limited to values within the design envelope. The design example used 39 plant models ($M = 39$) and 3 models ($n = 3$) for the interpolation process. The selection of $n = 3$ is a judgment factor based upon some preliminary analysis of the interpolation error.

Plant-model dynamics. The plant model is solved as a discrete state-space representation as follows:

$$\left. \begin{aligned} \mathbf{x}^*(p, k+1) &= \mathbf{\Phi}_x^*(p) \mathbf{x}^*(p, k) + \mathbf{\Gamma}_x^*(p) \mathbf{u}^*(p, k) \\ \mathbf{y}_x^*(p, k) &= \mathbf{C}_x^*(p) \mathbf{x}^*(p, k) + \mathbf{D}_x^*(p) \mathbf{u}^*(p, k) \end{aligned} \right\} \quad (13)$$

where $\mathbf{\Phi}_x^*$, $\mathbf{\Gamma}_x^*$, \mathbf{C}_x^* , and \mathbf{D}_x^* are interpolated matrices that are updated each iteration; \mathbf{x}^* is the ideal plant

state vector; \mathbf{y}_x^* is the ideal plant-model output vector; and \mathbf{u}_x^* is the ideal plant-model control (scalar for the controller in this paper). For implementation, equations (13) are solved in incremental form where the input is $\Delta \mathbf{u}_x^*$, which is defined as the difference between the values at two successive sampling times:

$$\Delta \mathbf{u}_x^*(p, k) = \mathbf{u}_x^*(p, k) - \mathbf{u}_x^*(p, k-1) \quad (14)$$

and the output is $\Delta \mathbf{y}_x^*$. Using the incremental implementation eliminates trimming problems because the incremental plant-model states are always zero during steady-state conditions. For the incremental implementation, the dynamics are assumed to be constant during each sample interval. The total output is then solved by accumulating all previous increments as follows:

$$\mathbf{y}_x^*(p, k) = \mathbf{y}_x^*(p, k-1) + \Delta \mathbf{y}_x^*(p, k) \quad (15)$$

Feed-Forward Gains

Reference 1 presents an optimal cost function that is quadratic in states, controls, and the feed-forward tracking error e_k^* , which is defined as

$$e^*(p, k) = \mathbf{H}_y \mathbf{y}_x^*(p, k) - y_z(p, k) \quad (16)$$

where \mathbf{H}_y is a matrix that allows a selected combination of plant-model outputs to track the command-model output at every instant of time. Two approaches for gain calculation are shown in reference 1. The first is a variable-gain approach (refs. 15, 16, and 18), and the second is a perfect tracking approach. The variable-gain approach generates an optimal gain schedule in which the gains are optimized over the entire flight envelope and are functions of measured parameters at each instant of time. In the variable-gain approach, there is a trade-off between feed-forward state variations, control variations, and tracking performance.

In this paper, the perfect tracking approach is used; that is, the optimal cost-function penalty weights on states and controls are zero. Feed-forward gains are generated to make e_k^* zero at all instants of time. The control law is in the following incremental form:

$$\begin{aligned} \Delta \mathbf{u}_x^*(p, k) &= -\mathbf{K}_x^*(p) \Delta \mathbf{x}^*(p, k) - \mathbf{K}_z(p) \Delta \mathbf{x}_z(p, k) \\ &\quad - \mathbf{K}_u(p) \Delta u_z(p, k) \end{aligned} \quad (17)$$

where \mathbf{K}_x^* is the plant-model state gains, \mathbf{K}_z is the command-model state gains, and \mathbf{K}_u is the command-model control input gain. (See fig. 2 for structure.) Equations (5) and (13) with \mathbf{D}_x^* assumed

zero, equation (16) with e_k^* equal to zero, and equation (17) give the perfect tracking feed-forward gains as

$$K_u(p) = -[\mathbf{H}_x^*(p) \mathbf{\Gamma}_x^*(p)]^{-1} \mathbf{C}_z(p) \mathbf{\Gamma}_z(p) \quad (18)$$

$$\mathbf{K}_z(p) = -[\mathbf{H}_x^*(p) \mathbf{\Gamma}_x^*(p)]^{-1} \mathbf{C}_z(p) \mathbf{\Phi}_z(p) \quad (19)$$

$$K_x^*(p) = -[\mathbf{H}_x^*(p) \mathbf{\Gamma}_x^*(p)]^{-1} \mathbf{H}_x^*(p) \mathbf{\Phi}_x^*(p) \quad (20)$$

with

$$\mathbf{H}_r^*(p) = \mathbf{H}_y \mathbf{C}_x^*(p) = [1 \ 1 \ 1] \mathbf{C}_x^*(p) \quad (21)$$

Equation (21) shows that the plant-model output is the sum of three regulated outputs that have been chosen to match the feedback controller. The variables in equations (18) to (21) are from the plant model and command model with the feed-forward gains calculated at each sampling interval. When \mathbf{D}_x^* is not zero, as with acceleration output, there is a small residual tracking error. However, \mathbf{D}_x^* is included in the dynamic equations for the plant model (eq. (13)). Because there is one feed-forward control, the matrix inversion in equations (18) to (20) is trivial. For two or three controls, the matrix inversion can still be accomplished reasonably fast.

Algorithm

The order in which equations are being implemented has been changed slightly from that shown in reference 1. The three main changes are as follows:

1. The command-model input uses total variables instead of incremental variables; thus, the output has total variables.
2. The total command-model output variable instead of the plant-model output variable is passed to the feedback controller.
3. The incremental plant-model control signal instead of the total plant-model control signal is passed to the feedback controller.

The first change was made because at the command model output during the accumulation process, the incremental version resulted in a significant error caused by the variable dynamics, which are assumed to be constant during each sampling interval. The second change was made to eliminate the need for an accumulator at the plant-model output because perfect tracking is used. An accumulator acts as a summing device and is similar to an integrator. This approach also eliminates the small error caused by the nonlinear implementation because \mathbf{D}_x^* in the

plant model is nonzero. Finally, the third change incorporates a limited accumulator in the feedback controller; thus, the need for a separate limited accumulator in the feed-forward controller is eliminated.

Starting with input $u_z(p, k)$, the algorithm is as follows:

1. Solve for the incremental input $\Delta u_z(p, k) = u_z(p, k) - u_z(p, k - 1)$.
2. Compute $\mathbf{\Phi}_z(p)$ in equation (8) and $\mathbf{\Gamma}_z(p)$ in equation (9). (Note $\mathbf{C}_z(p)$ is a constant matrix in this paper.)
3. Update the command-model dynamic equations (eqs. (5)).
4. Compute the incremental command-model state vectors $\Delta \mathbf{x}_z(p, k) = \mathbf{x}_z(p, k) - \mathbf{x}_z(p, k - 1)$.
5. Perform plant-model interpolation by using equations (10) to (12) for $\mathbf{\Phi}_x^*(p)$, $\mathbf{\Gamma}_x^*(p)$, $\mathbf{C}_x^*(p)$, and $\mathbf{D}_x^*(p)$.
6. Compute feed-forward gains with equations (18) to (21).
7. Solve for the incremental control (eq. (17)).
8. Update the plant-model dynamic equations (eqs. (13)) by using the incremental control input from step 7. (Note, the states and outputs are also incremental.)
9. Perform either step a or step b.
 - a. Solve equation (15) for $\mathbf{y}_x^*(p, k)$ and compute $\mathbf{H}_y \mathbf{y}_x^*(p, k)$ as in equation (16).
 - b. Use $y_z(p, k)$ for $\mathbf{H}_y \mathbf{y}_x^*(p, k)$ since for perfect tracking $e^*(p, k)$ is 0 (eq. (16)). The signal $y_{c,x}^*(p, k)$ can represent either the command-model output or the plant-model output. (This step was used in this example.)
10. Send variables $\Delta u_x^*(p, k)$, $y_{c,x}^*(p, k)$, and $\Delta \mathbf{y}_x^*(p, k)$ to the feedback controller.

Feedback Controller

Design of the feedback controller is described in references 18 and 19 and is also summarized in this section for completeness. Figure 8 shows the discrete PIF control structure that is used for design and linear analysis. The output feedback measurement vector \mathbf{y}_{rk} is input to both the proportional plus integral (PI) feedback paths, which are in parallel. The outputs from the PI structure go to a low-pass filter to produce the control position output u_{rk} . The PIF controller is a rate-command structure where the proportional feedback gain matrix $\mathbf{K}_{xp}(p)$, the integrator gain $K_{xI}(p)$, and the control filter gain $K_{xu}(p)$ all join at a summing junction to produce the

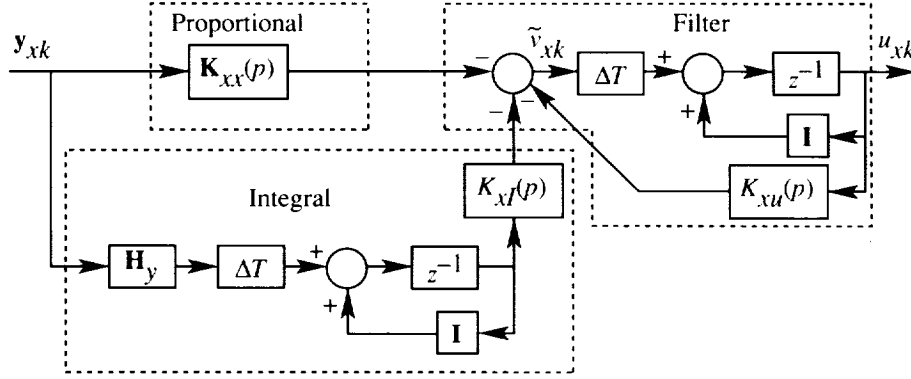


Figure 8. PIF feedback control structure for design and linear analysis.

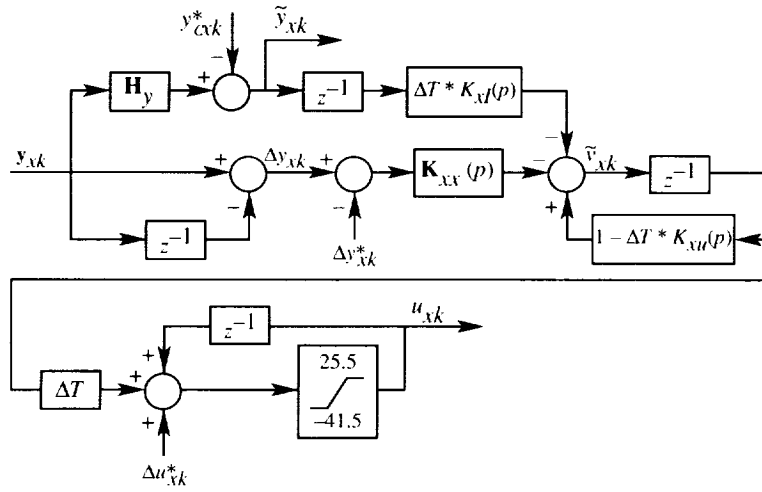


Figure 9. Feedback controller implementation.

rate command \tilde{v}_{xk} . The time step ΔT from \tilde{v}_{xk} to u_{xk} accommodates necessary computational delays. The regulated variables are defined by row vector \mathbf{H}_y as given in equation (21).

The feedback gain matrix has a linear, functional relationship with parameter p and contains both constant- and variable-gain parts that are implemented as

$$\mathbf{K}(p) = \mathbf{K}_0 + \sum_{i=1}^{n_p} p_i(\nu_i) \mathbf{K}_i \quad (22)$$

where the variable ν_i represents some measured variable that the designer selects for the gain-scheduling parameter and n_p is the number of gain-scheduling parameters. The relationship between p_i and ν_i can be either linear or nonlinear. The feedback gains in figure 8 are partitions of the overall gain matrix as

$$\mathbf{K}(p) = [\mathbf{K}_{xx}(p) \ K_{xI}(p) \ K_{xu}(p)] \quad (23)$$

The feedback controller was implemented incrementally with total measurable quantities. (See refs. 1, 3, and 26.) The advantage of the incremental implementation is that trim tables are not required; thus, the airplane automatically goes to a new equilibrium state as the integrated output follows the command. Because this controller is described in reference 19, only a few key equations are included here to show how the feed-forward signals are integrated into the feedback controller. Integration of the two controllers was found to be easy. (Some of the notation used in this paper differs from that used in ref. 19.)

As shown in figure 9, the rate command $\tilde{v}_x(p, k)$ is solved as

$$\begin{aligned} \tilde{v}_x(p, k) = & [\mathbf{I} - \Delta T K_{xu}(p)] \tilde{v}_x(p, k-1) \\ & - \mathbf{K}_{xx}(p) [\Delta y_x(p, k) - \Delta y_x^*(p, k)] \\ & - \Delta T K_{xI}(p) [\mathbf{H}_y y_x(p, k-1) - y_{cx}^*(p, k-1)] \end{aligned} \quad (24)$$

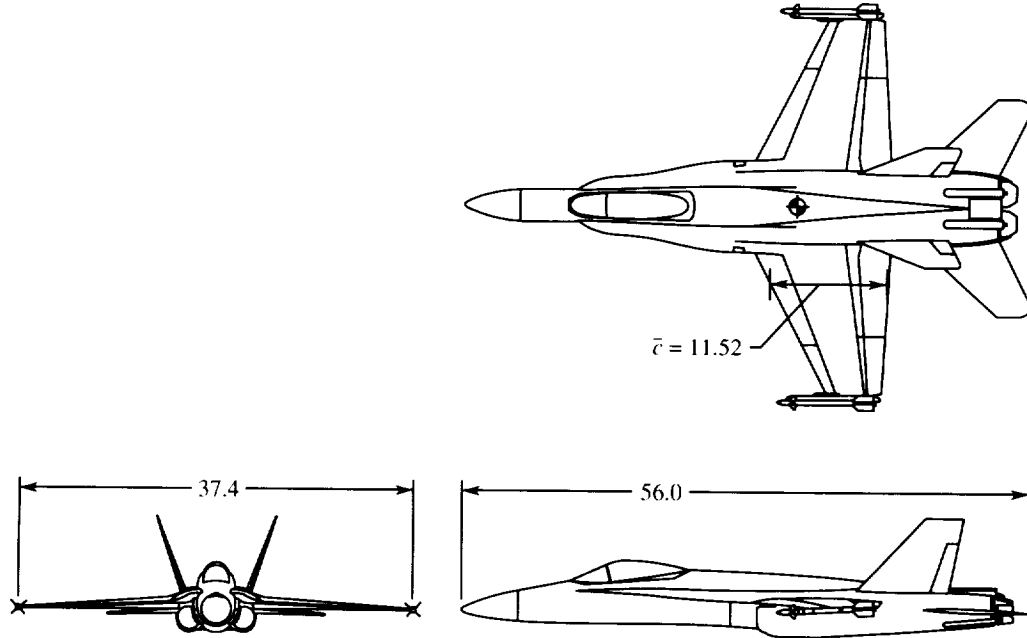


Figure 10. Major dimensions of HARV. All dimensions are in feet.

Then, $u_x(p, k)$ is calculated as

$$u_x(p, k) = u_x(p, k - 1) + \Delta u_x^*(p, k) + \Delta T \tilde{v}_x(p, k - 1) \quad (25)$$

where $\Delta y_x(p, k)$ is the incremental output feedback measurement vector. Equation (25) shows that $u_x(p, k)$ is a combination of the integral of $\tilde{v}_x(p, k)$ (delayed one time period) and the accumulated sum of the feed-forward incremental control signal $\Delta u_x^*(p, k)$.

Facilities

The SOFFT controller was applied to a nonlinear simulation model representing an F/A-18 airplane modified to have multiaxis thrust vectoring for additional pitch and yaw control. This modified configuration is known as the HARV (ref. 21). The F/A-18 airplane is a multirole fighter/attack airplane with supersonic dash capability and good low-speed high- α maneuvering capability. Major dimensions of the HARV are shown in figure 10. Thrust-vectoring capability was added to the basic F/A-18 aircraft by removing the secondary nozzles and adding three thrust-vectoring vanes per engine (fig. 11). The modified airplane has a nominal weight of almost 36 000 lb, which is approximately 4000 lb heavier than the basic F/A-18 aircraft.

The F/A-18 aircraft simulation on which the HARV model is based is discussed in detail in reference 27. The HARV simulation was built from fully nonlinear aerodynamic, engine, and control sys-

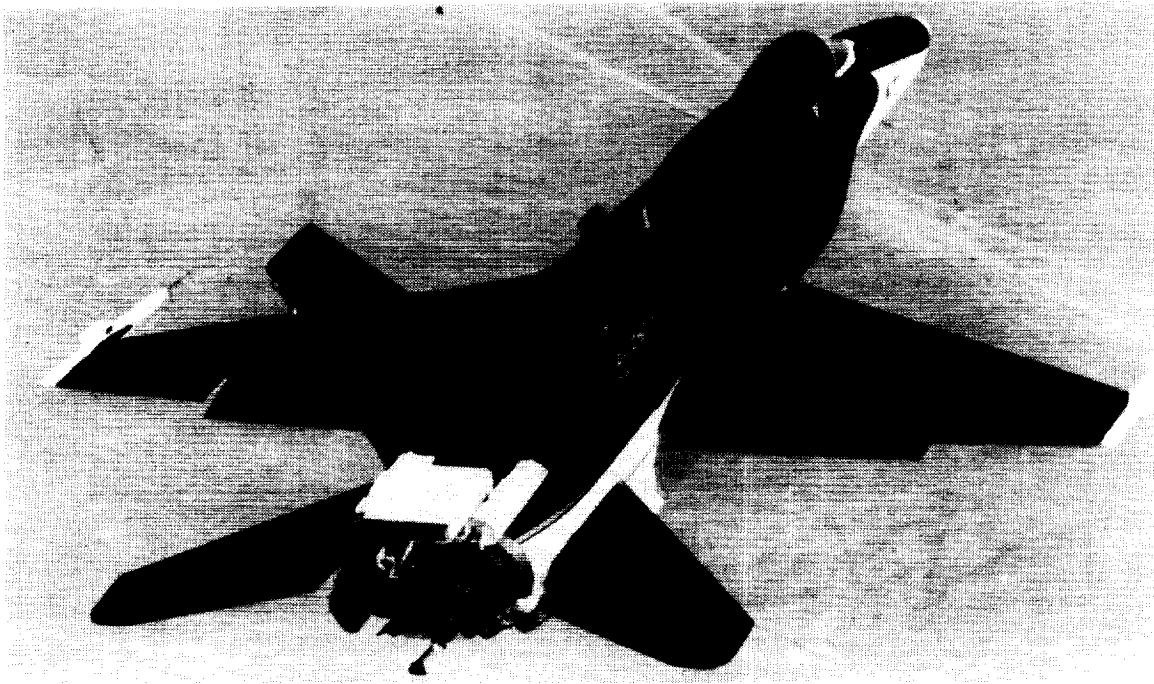
tem models of the production F/A-18 aircraft; these models were obtained from McDonnell Douglas Corporation. The McDonnell Douglas aerodynamic data base is for $\alpha = -10^\circ$ to 90° , sideslip $\beta = -20^\circ$ to 20° , altitudes to 60 000 ft, and speeds to Mach 2.0. Aerodynamic increments were added to the database because of the addition of thrust-vectoring vanes, actuator housings, and a spin parachute. Jet-induced effects were added for the change in airflow over the airframe that resulted from thrust vectoring.

The engine model, also obtained from McDonnell Douglas, incorporated thrust vectoring, the effects of Mach and altitude, and the dynamic response of engine thrust. Also included were the effects of α and vane deflection. Gross thrust and ram drag were tabulated separately; this tabulation allowed thrust vectoring to act on gross thrust only.

The SOFFT longitudinal control law discussed herein was integrated with a high- α lateral-directional controller to provide stability and maneuverability in the lateral-directional axes. The thrust-vectoring outputs from the two controllers go to a vane control system known as the mixer/predictor. The mixer/predictor converts pitch, yaw, and roll thrust vectoring commands into equivalent commands for the six thrust-vectoring vanes to yield the required jet deflection.

Simulation Results and Discussion

The SOFFT feed-forward controller was integrated with the HARV longitudinal controller



I-92-4360

Figure 11. HARV with thrust vectoring vanes.

(ref. 19) by inserting SOFFT between the command generator and feedback controller (fig. 1) and by eliminating the command generator tracker. This configuration was then tested in a nonlinear batch simulation to evaluate agility performance and tracking. Some specifics related to the feedback controller design and the results of the nonlinear batch simulations are described in this section.

Feedback Controller Specifics

In the variable-gain feedback design, six gain-schedule parameters $p_i(\nu_i)$ were used. These parameters are functions of α , Q_c , and P_s and were selected to cover independent degrees of freedom (α , speed, and altitude). The $p_i(\nu_i)$ and their limits were

$$\left. \begin{aligned}
 p_1 &= 0.1\alpha & (1.5 \leq \alpha \leq 65) \\
 p_2 &= 0.01Q_c & (10 \leq Q_c \leq 470) \\
 p_3 &= 0.001P_s & (498 \leq P_s \leq 1200) \\
 p_4 &= Q_c/P_s & (0.008 \leq p_4 \leq 0.4) \\
 p_5 &= 0.1\alpha - 3.5 & (\alpha > 35) \\
 p_5 &= 0 & (\alpha \leq 35) \\
 p_6 &= 0.01Q_c - 2.5 & (Q_c > 250) \\
 p_6 &= 0 & (Q_c \leq 250)
 \end{aligned} \right\} (26)$$

where the limits were selected to cover the HARV flight envelope. These p_i are used in equation (22) to calculate new feedback gains at each sample time.

The feedback gains changed continuously with the measured variables. The function was completely continuous and smooth except at two points. The first four parameters cover the entire HARV flight envelope; the last two parameters cover only portions of the envelope and were selected to tune in those portions of the design envelope. Parameter p_5 was used only when α is 35° or greater, and parameter p_6 was used when Q_c is 250 lb/ft^2 or greater. Both p_5 and p_6 have lower limits of zero and are not differentiable at the break points. When any value of ν_i exceeded the design limit, the variable was limited at the value shown in equation (26). The coefficients were selected to keep the $p_i(\nu_i)$ near unity.

Although it is not shown in figure 9, $u_x(p, k)$ splits into two commands. One command is position limited and goes directly to the stabilator input, while the other command passes through a limited washout filter and becomes the pitch thrust-vectoring command.

Agility

The simulation approach for agility performance evaluation is to first trim the airplane at a predetermined α (or Mach number) at $1g$ and $25\,000 \text{ ft}$.

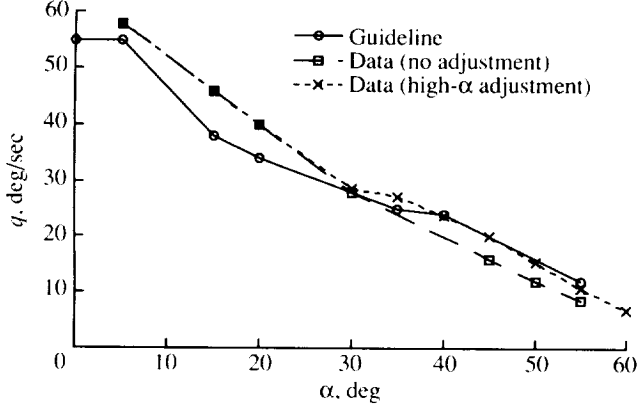


Figure 12. Pitch rate agility for various initial α trims at 25 000 ft.

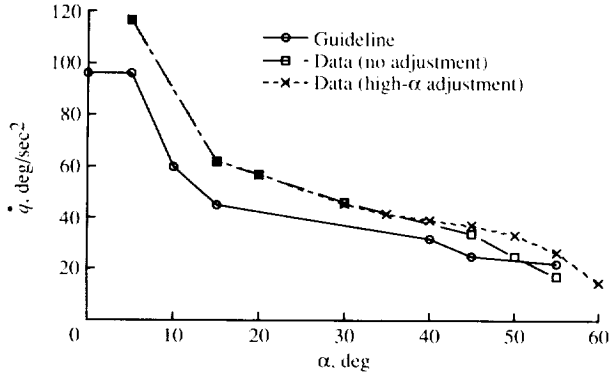


Figure 13. Pitch acceleration agility for various initial α trims at 25 000 ft.

At low- α conditions, the thrust available was sufficient to maintain a flight path angle of 0° . However, at a flight path angle of 35° or greater, maximum thrust was insufficient and resulted in a negative flight path angle. At time 0^+ , the throttle is moved to maximum (afterburner), 2 sec later full aft pitch stick (5-in. maximum) is applied, and the peak pitch acceleration and pitch rate are measured.

Figure 12 shows the pitch rate agility for various initial trim α 's, and figure 13 shows the pitch acceleration agility for the same conditions. In each figure, the solid line represents the guideline for desirable agility response (ref. 28) and the dashed lines represent controller performance. The two data plots deviate above $\alpha = 30^\circ$ where the high- α adjustment discussed previously is the only difference between the data of the command model with lower limit of 3 for ω_z and no adjustment and the data for the command model with the low-speed high- α adjustment for ω_z . The adjustment improves both pitch rate, q , and pitch acceleration, \dot{q} , agility. Pitch rate ei-

ther exceeds or meets the guideline at all α up to 45° , when the data becomes slightly lower than the guideline. Pitch acceleration with the high- α adjustment exceeds the guideline at all α and significantly exceeds the guideline at most α .

Tracking

Approximately 19 sec of pilot pitch stick input command δ_{sp} were extracted from a real-time simulation session during a tracking task for a different controller at approximately Mach 0.4 and an altitude of 25 000 ft. These data were then used in the nonlinear batch simulation to evaluate the SOFFT controller. Shortly after the start of the simulation run, the pilot slowly increased throttle to afterburner and reached maximum thrust in approximately 4 sec. The pilot also moved the lateral stick to roll the airplane to approximately 60° within the first 5 sec, and then maneuvered between 60° and 80° for the remainder of the simulation. Because this paper is for a longitudinal controller, only those variables relating to the longitudinal axis are described.

Figure 14 shows 10 time histories: δ_{sp} , u_{zk} , y_{crk}^* , ω_z , ζ_z , e_k^* , α , q , \tilde{y}_{rk} , and u_{rk} where arguments p and k are dropped for simplicity. The last four time histories (α , q , \tilde{y}_{rk} , and u_{rk}) show a comparison between the SOFFT controller response and the controller responses from reference 19. The first two time histories (δ_{sp} , u_{zk}) are identical for both controllers, and the third to sixth time histories (y_{crk}^* , ω_z , ζ_z , e_k^*) only apply to the SOFFT controller.

Signal u_{zk} has the same noise content as δ_{sp} , but it is larger in magnitude because of the command generator gains. Signal y_{crk}^* (step 9b of algorithm) illustrates the filtering within the command model. The plot of y_{crk}^* is clearly less noisy than that of u_{zk} , particularly at the high- α flight conditions, where ω_z is at or near the lower boundary of 3, and ζ_z is near its upper boundary of 1. The feed-forward tracking error e_k^* is relatively small (generally less than 0.1 percent of y_{crk}^*) and is caused by the assumption that \mathbf{D}_r^* (eqs. (13)) is 0 in the perfect tracking equations.

Because the feedback controller regulates the sum of measured signals α , q and n_z , α only approximates y_{crk}^* . In the nonlinear simulation, pitch rate output is modified (not shown in fig. 9 for simplicity) by nonlinear gravity compensation prior to use by the feedback controller. The feedback controller tracking error \tilde{y}_{rk} is defined as

$$\tilde{y}_{rk} = \mathbf{H}_y y_{rk} - y_{crk}^* = (\alpha + q + n_z)_k - y_{crk}^* \quad (27)$$

which is the integral term (one time step ahead) in equation (24). As shown in figure 14, \tilde{y}_{rk} has

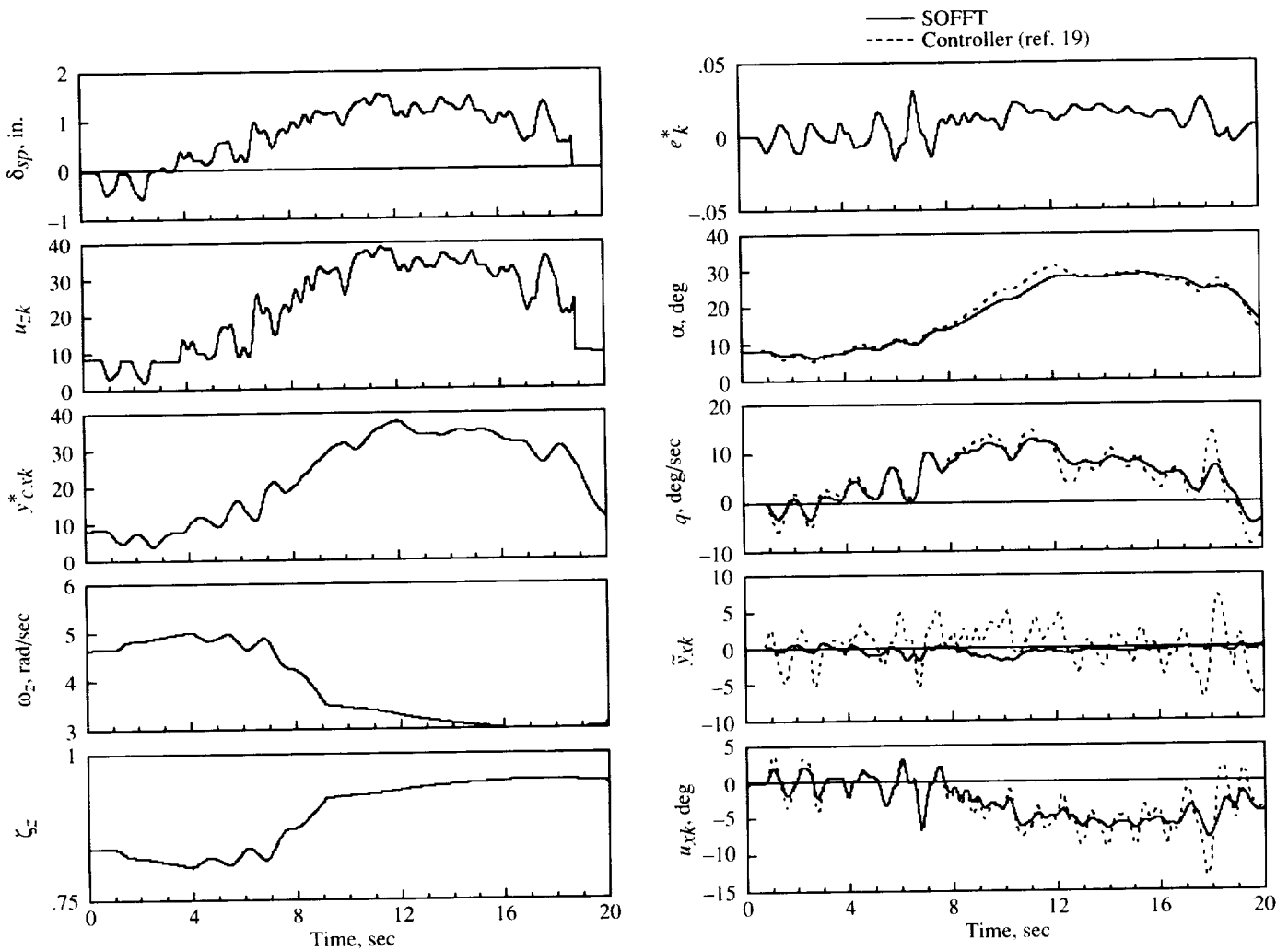


Figure 14. Tracking simulation. Mach = 0.45; h = 25 000 ft.

peaks of 1.6 for SOFFT and is generally below 1.0, which indicates improved feedback regulation compared to the reference 19 controller which has peaks that reach 7.5. Comparison between the SOFFT controller and the controller in reference 19 shows that SOFFT filters undesired pilot-induced frequencies much more effectively, which results in significantly reduced control-effector activity u_{xk} .

Concluding Remarks

This paper describes the design and evaluation of a stochastic optimal feed-forward and feedback technology (SOFFT) control structure with emphasis on the feed-forward controller. The feed-forward controller was designed separately with an objective of perfect tracking, and then it was easily integrated with a previously designed feedback controller with different objectives. The main compo-

nents of the feed-forward controller are the command model, plant model with interpolator, and feed-forward gains.

The command model incorporates variable dynamics for the command-model short-period frequency (ω_z) and the command-model short-period damping ratio (ζ_z), which are functions of angle of attack (α) and dynamic pressure (\bar{q}). In general, as speed increases at low α , ω_z increases and ζ_z goes to its lowest limit of 0.71. Design parameters have been chosen along the upper boundary of the level 1 flying qualities guidelines with a minimum ω_z of 3 to meet agility guidelines. At low dynamic pressure and high α ($\alpha > 30^\circ$), an adjustment was made to vary ω_z as a function of α and \bar{q} , with an upper limit of 5 to meet the high- α agility requirements. The largest damping ratio of 1 occurs during low-speed flight, which

is generally at high α because pilots prefer greater damping during this phase of flight.

A unique interpolation is used within the feed-forward controller to generate a plant model from a finite number of state-space design models that cover the flight envelope. A metric representing the distance in parameter space from the operating point to each design model is computed and used to scale an entire matrix. Precise accuracy is not required for the feed-forward task, so the main benefit is that this procedure is relatively fast compared with linear interpolation using three independent variables. Thirty-nine reference models were used in the design, and the three reference models closest to the measured operating condition were used for the interpolation process.

A perfect tracking algorithm was used for on-line calculation of the feed-forward gains. This algorithm was derived by solving for the optimal gains that make a selected combination of the plant-model outputs follow the command model output. The equations should be easy to calculate for as many as three controls. Integration of the feed-forward controller with the feedback controller by using the SOFFT structure and an incremental implementation was straightforward.

Nonlinear batch simulation results show that use of the SOFFT controller enables agility guidelines for pitch rate and acceleration to be met. Without the high- α adjustment, pitch rate agility was slightly below the guideline for $\alpha > 30^\circ$.

Tracking task time history plots comparing the SOFFT controller with another controller with the same feedback system shows that SOFFT filters undesired pilot input frequencies much more effectively, has a smaller tracking error, and has reduced control-surface activity. Real-time and full-scale flight test pilot evaluations are still needed to determine flying qualities and tracking performance.

NASA Langley Research Center
Hampton, VA 23681-0001
March 31, 1994

References

1. Halyo, Nesim; Direskeneli, Haldun; and Taylor, Deborah B.: *A Stochastic Optimal Feedforward and Feedback Control Methodology for Superagility*. NASA CR-4471, 1992.
2. Stengel, R. F.; Broussard, J. R.; and Berry, P. W.: *The Design of Digital-Adaptive Controllers for VTOL Aircraft*. NASA CR-144912, 1975.
3. Broussard, J. R.; Berry, P. W.; and Stengel, R. F.: *Modern Digital Flight Control System Design for VTOL Aircraft*. NASA CR-159019, 1979.
4. Downing, D. R.; Bryant, W. H.; and Ostroff, A. J.: Flight Test of a VTOL Digital Autoland System Along Complex Trajectories. *A Collection of Technical Papers AIAA Guidance and Control Conference*, Aug. 1979, pp. 54-63. (Available as AIAA Paper 79-1703.)
5. Halyo, Nesim: *Development of a Digital Automatic Control Law for Steep Glideslope Capture and Flare*. NASA CR-2834, 1977.
6. Halyo, Nesim: *Terminal Area Automatic Navigation, Guidance, and Control Research Using the Microwave Landing System (MLS). Part 5 Design and Development of a Digital Integrated Automatic Landing System (DIALS) for Steep Final Approach Using Modern Control Techniques*. NASA CR-3681, 1983.
7. Halyo, Nesim: *Flight Tests of the Digital Integrated Automatic Landing System (DIALS)*. NASA CR-3859, 1984.
8. Halyo, Nesim; and Broussard, John R.: A Convergent Algorithm for the Stochastic Infinite-Time Discrete Optimal Output Feedback Problem. *Proceedings of the 1981 Joint Automatic Control Conference, Volume 1*, American Automatic Control Council, 1981, paper WA-1E.
9. Halyo, Nesim; and Broussard, John R.: *Investigation, Development, and Application of Optimal Output Feedback Theory. Volume I A Convergent Algorithm for the Stochastic Infinite-Time Discrete Optimal Output Feedback Problem*. NASA CR-3828, 1984.
10. Ostroff, A. J.; and Hueschen, R. M.: *Reconfigurable Multivariable Control Law for Commercial Airplane Using a Direct Digital Output Feedback Design*. NASA TM-85759, 1984.
11. Ostroff, A. J.; and Hueschen, R. M.: Investigation of Control Law Reconfigurations To Accommodate a Control Element Failure on a Commercial Airplane. American Control Conference, American Automatic Control Council, June 1984.
12. Ostroff, A. J.: Techniques for Accommodating Control Effector Failures on a Mildly Statically Unstable Airplane. American Control Conference, Institute of Electrical and Electronics Engineers and American Automatic Control Council, June 1985.
13. Belcastro, Christine M.; and Ostroff, Aaron J.: *Total Energy-Rate Feedback for Automatic Glide-Slope Tracking During Wind-Shear Penetration*. NASA TP-2412, 1985.
14. Halyo, Nesim; and Broussard, John R.: Algorithms for Output Feedback, Multiple Model and Decentralized Control Problems. NASA CP-2296, 1983, pp. 281-304.
15. Halyo, Nesim; Moerder, Daniel D.; Broussard, John R.; and Taylor, Deborah B.: *A Variable-Gain Output Feedback Control Design Methodology*. NASA CR-4226, 1989.
16. Halyo, Nesim: A Variable-Gain Output Feedback Control Design Approach. *A Collection of Technical Papers*,

Part 2—AIAA Guidance, Navigation and Control Conference, Aug. 1989, pp. 1238-1248. (Available as AIAA-89-3575-CP.)

17. Moerder, Daniel D.; Halyo, Nesim; Broussard, John R.; and Caglayan, Alper K.: Application of Precomputed Control Laws in a Reconfigurable Aircraft Flight Control System. *J. Guid., Control, & Dyn.*, vol. 12, May-June 1989, pp. 325-333.
18. Ostroff, Aaron J.: High-Alpha Application of Variable-Gain Output Feedback Control. *J. Guid., Control, & Dyn.*, vol. 15, Mar.-Apr. 1992, pp. 491-497.
19. Ostroff, Aaron J.; and Proffitt, Melissa S.: *Longitudinal Control Design Approach for High-Angle-of-Attack Aircraft*. NASA TP-3302, 1993.
20. Ostroff, Aaron J.; Hoffler, Keith D.; and Proffitt, Melissa S.: High-Angle-of-Attack Research Vehicle (HARV) Longitudinal Controller: Design, Analyses, and Simulation. NASA TP-3446, 1994.
21. Matheny, Neil W., compiler: *High-Angle-of-Attack Projects and Technology Conference, Volume 1*. NASA CP-3137, 1992.
22. Wendel, Thomas R.: Flight Control Synthesis To Meet Flying Qualities Specifications: An Evaluation of Multivariable Synthesis Techniques. AIAA-87-2880, Sept. 1987.
23. Thompson, Clay M.; Coleman, Edward E.; and Blight, James D.: Integral LQG Controller Design for a Fighter Aircraft. AIAA-87-2452, Aug. 1987.
24. Military Standard Flying Qualities of Piloted Aircraft. MIL-STD-1797A, Jan. 30, 1990.
25. Wilson, David J.; and Riley, David R.: *Flying Qualities Criteria Development Through Manned Simulation for 45° Angle of Attack—Final Report. Volume I Simulation Results and Analysis*. NASA CR-4435, Vol. I, 1992.
26. Maybeck, Peter S.: *Stochastic Models, Estimation, and Control, Volume 3*. Academic Press, 1982.
27. Buttrill, Carey S.; Arbuckle, P. Douglas; and Hoffler, Keith D.: *Simulation Model of a Twin-Tail, High Performance Airplane*. NASA TM-107601, 1992.
28. Foster, John V.; Bundick, W. T.; and Pahle, Joseph W.: Controls for Agility Research in the NASA High-Alpha Technology Program. SAE Paper 912148, Sept. 1991.



REPORT DOCUMENTATION PAGE			Form Approved OMB No. 0704-0188	
Public reporting burden for this collection of information is estimated to average 1 hour per response, including the time for reviewing instructions, searching existing data sources, gathering and maintaining the data needed, and completing and reviewing the collection of information. Send comments regarding this burden estimate or any other aspect of this collection of information, including suggestions for reducing this burden, to Washington Headquarters Services, Directorate for Information Operations and Reports, 1215 Jefferson Davis Highway, Suite 1204, Arlington, VA 22202-4302, and to the Office of Management and Budget, Paperwork Reduction Project (0704-0188), Washington, DC 20503.				
1. AGENCY USE ONLY (Leave blank)	2. REPORT DATE June 1994	3. REPORT TYPE AND DATES COVERED Technical Paper		
4. TITLE AND SUBTITLE Design and Evaluation of a Stochastic Optimal Feed-Forward and Feedback Technology (SOFFT) Control Architecture			5. FUNDING NUMBERS WU 505-64-30-01	
6. AUTHOR(S) Aaron J. Ostroff and Melissa S. Proffitt				
7. PERFORMING ORGANIZATION NAME(S) AND ADDRESS(ES) NASA Langley Research Center Hampton, VA 23681-0001			8. PERFORMING ORGANIZATION REPORT NUMBER L-17273	
9. SPONSORING/MONITORING AGENCY NAME(S) AND ADDRESS(ES) National Aeronautics and Space Administration Washington, DC 20546-0001			10. SPONSORING/MONITORING AGENCY REPORT NUMBER NASA TP-3419	
11. SUPPLEMENTARY NOTES Ostroff: Langley Research Center, Hampton, VA; Proffitt: Lockheed Engineering & Sciences Company, Hampton, VA.				
12a. DISTRIBUTION/AVAILABILITY STATEMENT Unclassified Unlimited Subject Category 08			12b. DISTRIBUTION CODE	
13. ABSTRACT (Maximum 200 words) This paper describes the design and evaluation of a stochastic optimal feed-forward and feedback technology (SOFFT) control architecture with emphasis on the feed-forward controller design. The SOFFT approach allows the designer to independently design the feed-forward and feedback controllers to meet separate objectives and then integrate the two controllers. The feed-forward controller has been integrated with an existing high-angle-of-attack (high- α) feedback controller. The feed-forward controller includes a variable command model with parameters selected to satisfy level 1 flying qualities with a high- α adjustment to achieve desired agility guidelines, a nonlinear interpolation approach that scales entire matrices for approximation of the plant model, and equations for calculating feed-forward gains developed for perfect plant-model tracking. The SOFFT design was applied to a nonlinear batch simulation model of an F/A-18 aircraft modified for thrust vectoring. Simulation results show that agility guidelines are met and that the SOFFT controller filters undesired pilot-induced frequencies more effectively during a tracking task than a flight controller that has the same feedback control law but does not have the SOFFT feed-forward control.				
14. SUBJECT TERMS Control; Feed-forward; Optimal; SOFFT			15. NUMBER OF PAGES 19	
			16. PRICE CODE A03	
17. SECURITY CLASSIFICATION OF REPORT Unclassified	18. SECURITY CLASSIFICATION OF THIS PAGE Unclassified	19. SECURITY CLASSIFICATION OF ABSTRACT	20. LIMITATION OF ABSTRACT	